Supercapacitors and Battery Energy Management based on New European Driving Cycle

Mamadou Baïlo Camara, Brayima Dakyo, Hamid Gualous

Journal of Energy and Power Engineering 6 (2012) 168-177

Supercapacitors and Battery Energy Management Based on New European Driving Cycle

Mamadou Baïlo Camara[1], Brayima Dakyo[1] and Hamid Gualous[2]

1. GREAH Laboratory, Technical Sciences Faculty, University of Havre, Le Havre 76058, France

2. LUSAC Laboratory, University of Caen, Cherbourg-Octeville 50100, France

Received: December 09, 2010 / Accepted: May 31, 2011 / Published: February 29, 2012.

Abstract: This paper presents a new strategy of embedded energy management between battery and supercapacitors (SC) for hybrid electric vehicles (HEV) applications. This proposal is due to the present trend in the field, knowing that the major drawback of the HEV is the autonomy problem. Thus, using supercapacitors and battery with a good energy management improves the HEV performances. The main contribution of this paper is focused on DC-bus voltage and currents control strategies based on polynomial controller. These strategies are implemented in PIC18F4431 microcontroller for DC/DC converters control. Due to reasons of cost and available components (no optimized), such as the battery and power semiconductors (IGBT), the experimental tests are carried out in reduced scale (2.7 kW). Through some simulations and experimental results obtained in reduced scale, the authors present an improved energy management strategy for HEV.

Key words: Battery, electric machine, energy storage, supercapacitors, polynomial control, hybrid electric vehicles, DC/DC converter.

1. Introduction

Today, the hybrid electric vehicles (HEV) including the supercapacitors and the battery or fuel-cell [1] are considered as a solution to embedded energy and environmental problems. These vehicles present the advantages of thermal vehicles (autonomy and flexibility in use) and electric ones (no pollution), but it is not the combination of these ones, because the components must be optimized. Due to energetic autonomy problem, the traction batteries used until now must be improved for future vehicles applications; and they must be dimensioned to satisfy the requested energy by the vehicle during transient states. In this context, an association of the batteries and the supercapacitors with a good energy management presents a promising solution in short time. This idea is due to supercapacitors dynamics behavior, their lifetime about 10 years and their high power density compared to batteries ones [2-5].

This paper proposes a new approach of energy management, related to currents and DC-bus voltage control, based on polynomial controllers. The polynomial control method gives a robust algorithm, with good performances in the following case of process: with a pure delay, whose dynamic characteristics change during operation, and where the reference should not be exceeded. To evaluate this approach, the hybrid system presented in Fig. 1 is used. This topology includes a battery's module, the supercapacitors (SC), an electric load (electric machine with inverter), and DC/DC converters. To validate the proposed method, some simulations and experimental tests are carried out in reduced scale. The control algorithms are implemented in a PIC18F4431 microcontroller for buck-boost converter control in SC side, and boost converter control

Corresponding author: Mamadou Baïlo Camara, associate professor, research fields: supercapacitors and battery modeling, energy management for transport and renewable energy applications. E-mail: camaram@univ-lehavre.fr.

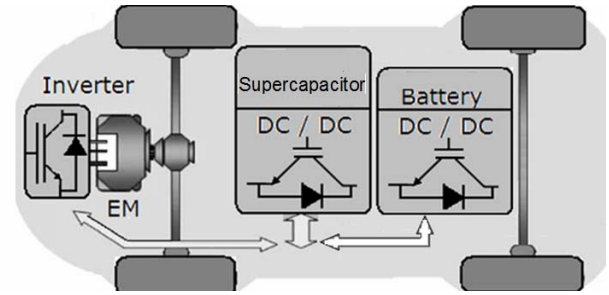

Fig. 1 Hybrid electric vehicles based on SC and battery.

in battery's side. The experimental data acquisition system is monitored using Labview software with PXI station.

2. Supercapacitors Characterization

To use supercapacitors as energy storage device in electric hybrid vehicles, it is necessary to connect several cells in series and/or in parallel to obtain a high voltage level. The proposed model of the SC, Fig. 2, includes an equivalent resistor R, and an equivalent capacitor including two components. The first component $\beta.V(t)$ has a linearly behavior with SC module voltage, and the second component C_0 is a constant capacitor [6]. This model describes the SC behavior during the charge and discharge operations.

To estimate the supercapacitors (SC) parameters, a module, including 20 cells of 3000 F-2.7 V in series with a maximum voltage of 54 V, is used. The parameters estimation method is based on an analysis of the experimental discharge curves at constant current. The experimental voltage measured during the SC module discharge at 100 A is presented in Fig. 3. The early discharge of the module is characterized by a voltage drop ΔV_0 in equivalent resistor R. This last can be estimated as presented in Eq. (1), where R_{sc}, and R_{con} are respectively the supercapacitors cells resistor and electric wiring resistor for SC module. The assumed linear behavior of the differential capacitor $C_0+\beta.V(t)$ enables to estimate k_0 coefficient, from experimental curve as plotted in Fig. 3.

$$R = R_{sc} + R_{con} = \frac{\Delta V_0}{I_{sc}}, \quad \Delta V_0 = V_0 - V_1 \qquad (1)$$

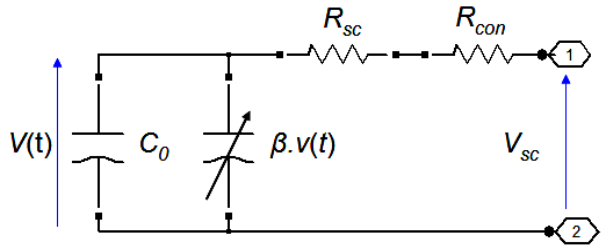

Fig. 2 Supercapacitors behavior model.

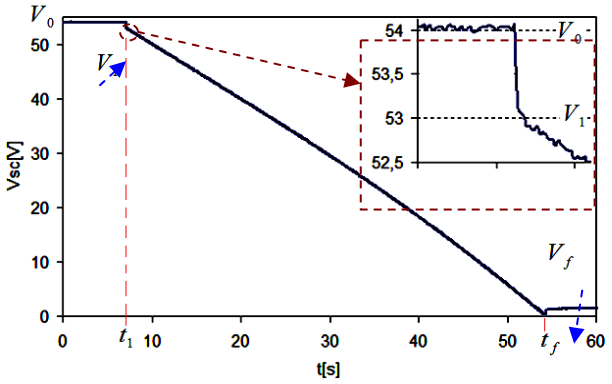

Fig. 3 Supercapacitors experimental voltage for I_{sc} = 100 A.

The resulting equation from this approximation is presented in Eq. (2).

$$k_0 \approx \left|\frac{V_f - V_1}{t_f - t_1}\right| = \left|\frac{0.55 - 53.11}{54 - 7.14}\right| \approx 1.123\ V/s \qquad (2)$$

The specific capacitor β, and constant component C_0, resulting from experimental curves analysis can be estimated as presented in Eq. (3). In this equation, $\Delta t = t_f - t_1$ presents the SC module discharge time in (s). In this equation, V_0 and $\Delta Vt = V_1 - V_f$ present respectively, the SC module initial voltage and module's voltage variation between V_1 and final voltage V_f.

$$\begin{cases} \beta = \left(\frac{1}{k_0} - \frac{\Delta t}{\Delta Vt}\right) \cdot \frac{I_{sc}}{2 \cdot V_0 - 0.5 \cdot \Delta Vt} \\ C_0 = \left(\frac{1}{k_0} - \left(\frac{1}{k_0} - \frac{\Delta t}{\Delta Vt}\right) \cdot \frac{2 \cdot V_1}{2 \cdot V_0 - 0.5 \cdot \Delta Vt}\right) \cdot I_{sc} \end{cases} \qquad (3)$$

To validate the model, the supercapacitors module is charged until maximal voltage, and discharged with pulsed current as plotted in Fig. 4. The simulation and experimental curves obtained from supercapacitors module characterization are compared in Fig. 5. These results show that the proposed model has a good behavior with pulsed current.

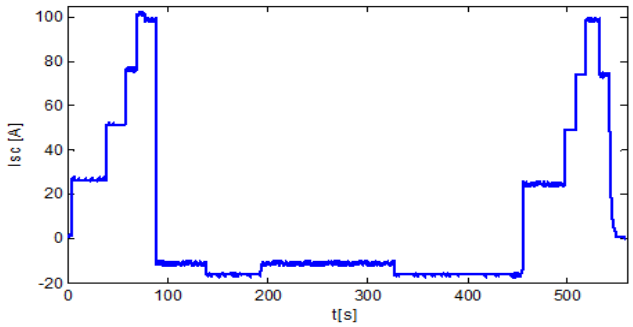

Fig. 4 Supercapacitors experimental current for charge and discharge operations.

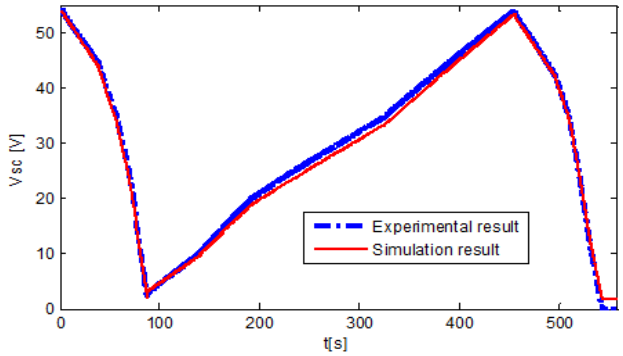

Fig. 5 SC module experimental and simulation voltage for charge and discharge operations.

In other words, the simulations and experimental results are very close. The SC module parameters (*R*, C_0 and β) obtained from experimental results of 20 cells of BCAP3000P type are presented in Table 1. However, some parameters such as *R* and C_0 have needed some adjustments after several cycles of the charge-discharge, i.e., after some years of use.

3. DC/DC Converters and HEV Modeling

The SC and battery's modules are connected on DC-bus through two buck-boost converters, which ensure the energy exchange between these storage devices as presented in Fig. 6. The control strategies [7-10] of these converters must be developed as function of the requested energy by the hybrid electric vehicles.

3.1 Buck-Boost Converters Modeling

To establish an analytical model of the buck-boost converters, it is necessary to analyze the two operations modes (buck and boost). During boost operation mode,

Table 1 Supercapacitors module parameters.

Symbol	Name	Value
R	SC module resistance	9.4 mΩ
C_0	SC module constant capacitance	86.6 F
β	SC module specific capacitance	0.04 F/V
V_o	SC module initial voltage	54 V

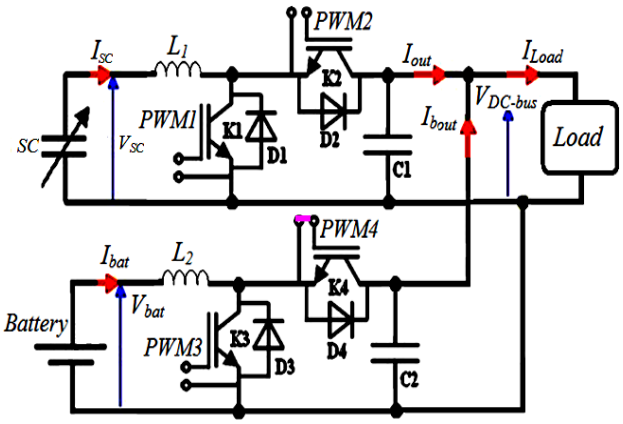

Fig. 6 Supercapacitors and battery connection topology.

Fig. 6, K_1 semiconductor is *ON*, and K_2 is *OFF*. In this case, the SC module provides the traction energy to HEV. In the buck mode, K_2 is *ON* and K_1 pass to *OFF*; the SC module stores energy from DC-bus (braking energy). The analytical model of the buck-boost converter in SC side resulting from the sequences analyzes is given in Eq. (4), where, *k* and u_2 define the sign of the SC current, and the equivalent value of the duty cycle. In battery side, only the boost converter mode is considered in this paper. In this case, the converter average model obtained from the sequences analyzes is presented in Eq. (5),

$$\begin{cases} V_{L1} = L_1 \cdot \dfrac{d}{dt}(I_{sc}) = k \cdot (V_{sc} - u_2 \cdot V_{DC-bus}) \\ I_{load} = I_{bout} + k \cdot I_{out} \end{cases} \tag{4}$$

$$\begin{cases} V_{L2} = L_2 \cdot \dfrac{d}{dt}(I_{bat}) = \delta \cdot (V_{bat} - u \cdot V_{DC-bus}) \\ I_c = (C_1 + C_2) \cdot \dfrac{d}{dt}(V_{DC-bus}) \approx u \cdot I_{bat} - I_{bout} \\ u = 1 - \alpha' \end{cases} \tag{5}$$

where δ and *u* present also the sign of the battery's current I_{bat} and the equivalent value of the duty cycle. These average models have a nonlinear behavior due to crosses between the control variables (u_2, *u*), and the state variables (I_{sc}, I_{bat}, V_{DCbus}). In more of this

constraint, the following variables: $V_{DC\text{-}bus}$, V_{sc}, I_{Load} and V_{bat} are likely to disturb the control; they must be measured and used in control law estimation to ensure a good dynamics of control [11].

3.2 Electric Vehicle Dynamic Modeling

The dynamic model of HEV presents a total effort, which must be compensated by the vehicle's motor to move forward. This global effort presented in Eq. (6) includes four components studied in Refs. [12, 13].

$$F_{te} = F_{rr} + F_{hc} + F_{aero} + F_{acc} \tag{6}$$

In this equation, F_{rr} is the rolling resistance force, F_{hc} is the hill climbing force, F_{aero} is the aerodynamic force, and F_{acc} is the acceleration force.

This Eq. (6) gives an electric power transmitted to wheels. The electric load current profile, obtained from power balances between inverter's input and output, is expressed in Eq. (7). In this paper, the road is considered flat, the mass of the vehicle is 800 kg, and inverter's efficiency η is fixed at 75%.

$$I_{Load} = \frac{v}{\eta . V_{DCbus}} \cdot F_{te} \tag{7}$$

4. Converters Control Strategy

The converters control strategy is based on the polynomial controllers implemented in Matlab for energy management between DC-bus and hybrid sources (battery and supercapacitors). This strategy includes two steps: the first is based on supercapacitors current control, and the second is focused on DC-bus voltage control with the battery's current control through an inner loop.

4.1 Supercapacitors Current Control Strategy

To control the SC current, the bidirectional converter control laws obtained from buck-boost converter modeling are used. These control laws are presented in Eq. (8) for buck mode, and in Eq. (9) for boost mode.

$$\alpha = \alpha_{buck} = \frac{V_{sc} + V_{L1}}{V_{DC-bus}}, \quad k = -1 \tag{8}$$

$$\alpha = \alpha_{boost} = 1 - \frac{V_{sc} - V_{L1}}{V_{DC-bus}}, \quad k = 1 \tag{9}$$

The SC reference current I_{scref} established from electric power balances between buck-boost converters input and output is showed in Eq. (10). In this equation, I_{load} presents the load current, and I_{batref} is the battery's reference current obtained from DC-bus voltage control. This last will be presented in next paragraph.

$$I_{scref} \approx \frac{V_{DC-bus}}{V_{sc}} \cdot I_{load} - \frac{V_{bat}}{V_{sc}} \cdot I_{batref} \tag{10}$$

The proposed control strategy of the SC current is illustrated in Fig. 7, where an anti-windup loop is added in V_{L1} voltage estimation loop to improve the supercapacitors current control performances.

4.2 DC-Bus Voltage Control Strategy

The boost converter control law established from Eq. (5) for the DC-bus voltage managing is given in Eq. (11). In this case, the cascaded control loops are necessary: an inner loop for battery's current control and outside loop for DC-bus voltage ones.

$$\alpha' = 1 - \frac{V_{bat} - V_{L2}}{V_{DC-bus}}, \delta = 1 \tag{11}$$

The battery's reference current I_{batref} estimated from electric powers balances between boost converter input and output is presented in Eq. (12), where I_{bout} is the boost converter output current, and I_c is the DC-bus capacitor's current.

$$I_{batref} \approx \frac{V_{DC-bus}}{V_{bat}} (I_{bout} + I_c) \tag{12}$$

The DC-bus voltage control strategy is illustrated in Fig. 8 for the outer loop, and the inner loop is presented in Fig.9. To improve the voltage control performances, an anti-windup loop is added in DC-bus voltage control loop as expressed in Eq. (13), where I_{batref} is the battery's reference current.

$$\Delta I_c = \frac{\Delta I_{batref} \cdot V_{bat}}{V_{DC-bus}} - I_{bat} \tag{13}$$

4.3 Polynomials Controllers Coefficients Estimation

To obtain a minimal static error with disturbance rejection, $R(z)$ and $S(z)$ polynomials are selected as

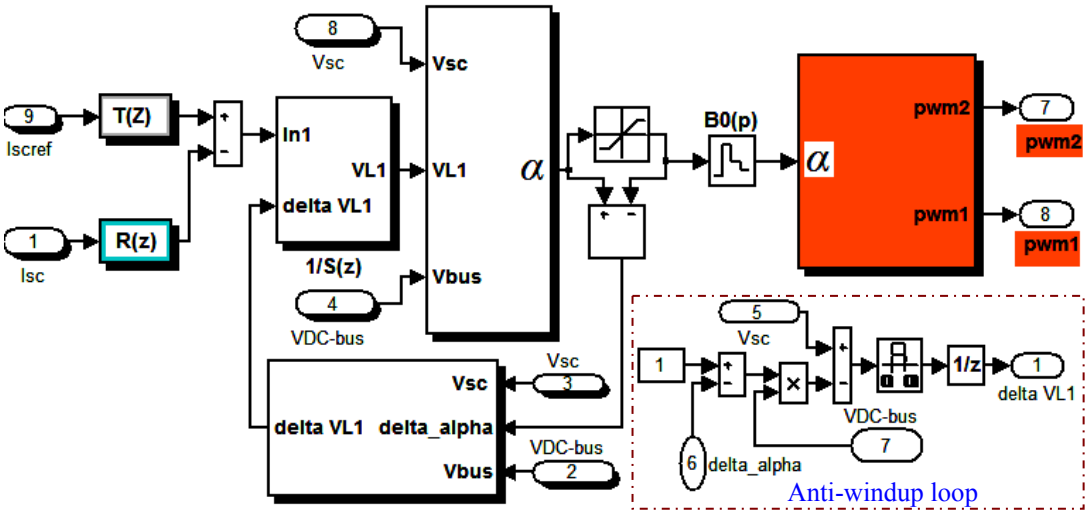

Fig. 7 Supercapacitors current control loop for charge and discharge operations.

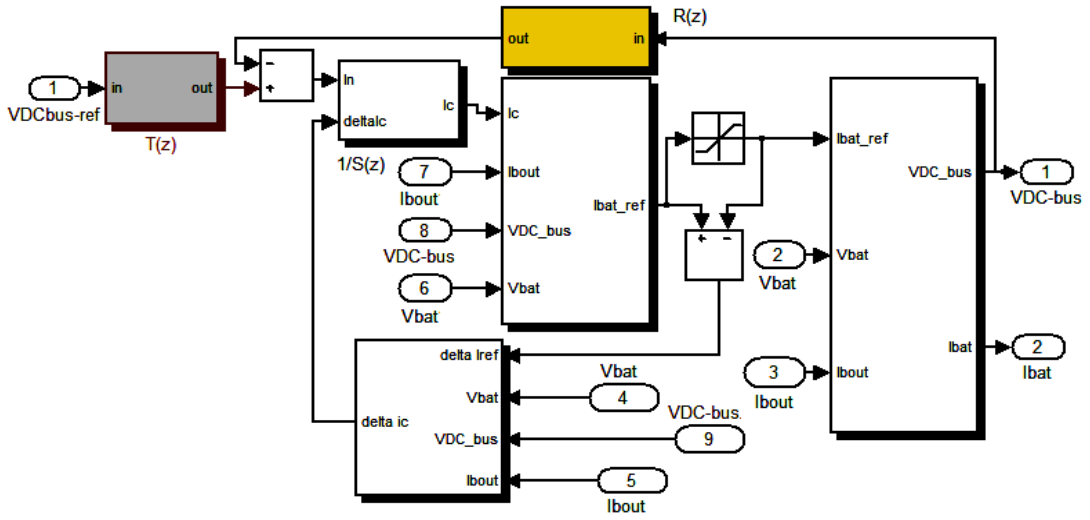

Fig. 8 DC-bus voltage control loop (outer loop).

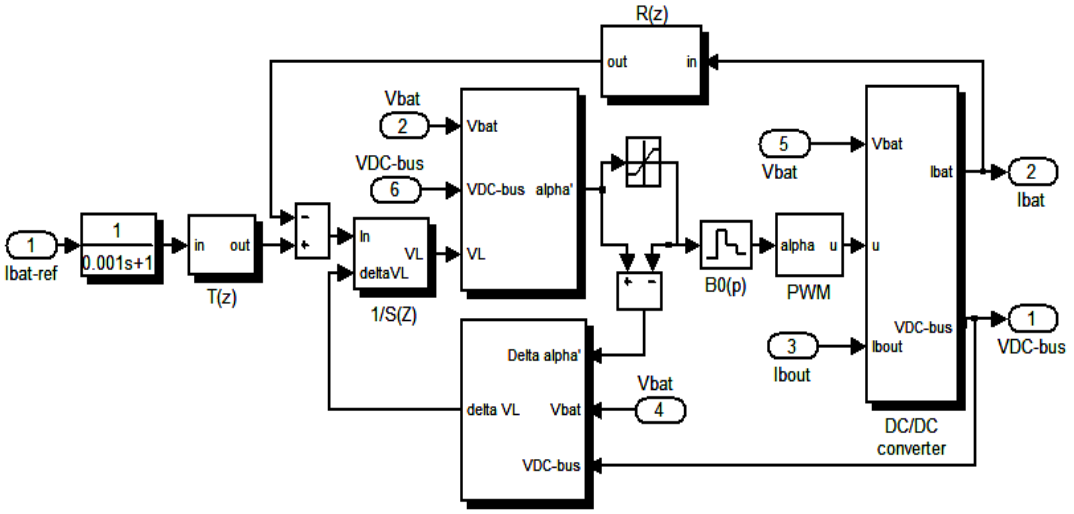

Fig. 9 Battery's current control loop (inner loop).

expressed in Eq. (14) [14]. The used method is described in previous papers [15], where a similar polynomial control strategy was employed for current control in the parallel topology of the DC/DC converter. In this paper, this technique will be applied to the buck-boost and boost converters for currents and DC-bus voltage control respectively. In Eq. (14), *xx* index correspond to *i* for currents control loops, and *v* for DC-bus voltage control ones.

$$\begin{cases} S(z) = 1 - z^{-1} \\ R(z) = r_{0xx} + r_{1xx} \cdot z^{-1} \end{cases}, \quad T(z) = R(z) \qquad (14)$$

The coefficients of the polynomials obtained from SC and battery's currents closed loops analysis is presented in Eq. (15). In this equation, T_e is the sampling period (100 µs); ω_i is the currents control band-width (selected maximum frequency of the band-width is lower than 1/10 of the IGBT control frequency); L_{yy} presents the SC and battery's currents smoothing inductors, where *yy = 1* for I_{sc}; and *yy = 2* for battery's current I_{bat}.

$$\begin{cases} r_{0i} = 2 \cdot \left(1 - \exp(-\omega_i \cdot T_e)\right) \cdot \dfrac{L_{yy}}{T_e} \\ r_{1i} = \left(\exp(-2 \cdot \omega_i \cdot T_e) - 1\right) \cdot \dfrac{L_{yy}}{T_e} \end{cases}, \omega_i \le \frac{2 \cdot \pi \cdot f_d}{10} \qquad (15)$$

The voltage control parameters obtained from DC-bus voltage closed loop is given in Eq. (16), where C_T is the *DC-bus* voltage smoothing capacitor, and ω_v is the voltage control band-width.

$$\begin{cases} r_{0v} = 2 \cdot \left(1 - \exp(-\omega_v \cdot T_e)\right) \cdot \dfrac{C_T}{T_e} \\ r_{1v} = \left(\exp(-2 \cdot \omega_v \cdot T_e) - 1\right) \cdot \dfrac{C_T}{T_e} \end{cases}, \begin{cases} \omega_v = 100 \cdot \omega_i \\ C_T = C_1 + C_2 \end{cases} \qquad (16)$$

The used parameters in current and voltage control loops are respectively presented in Eq. (17).

$$\begin{cases} r_{0i} + r_{1i} \cdot z^{-1} = 0.639 - 0.5879 \cdot z^{-1} \\ r_{0v} + r_{1v} \cdot z^{-1} = 264 - 132 \cdot z^{-1} \end{cases} \qquad (17)$$

These coefficients are estimated from following parameters:

- DC-bus capacitors : $C_1 = 1500\ \mu F$, $C_2 = 6800$ µF;
- I_{sc} and I_{bat} smoothing inductors : $L_1 = 2\ L_2 = 100$ µH;
- Currents loops band-width: $\omega_i = 1740$ *rad/s*;
- *DC-bus* voltage loop band-width: $\omega_v = 174000$ rad/s;
- Converters control frequency: $f_d = 2770$ Hz.

5. HEV Behavior Simulation Results

For these simulations, DC-bus voltage reference is fixed at constant value so that the SC module provides HEV energy request during the transient states. The load current I_{Load} profile is generated from HEV speed as expressed in Eq. (7). For hybrid system [16, 17] simulations, the HEV speed profile is plotted in Fig. 10. Fig. 11 shows the supercapacitors module voltage; this curve shows that the SC module charges and discharges as function of supercapacitors current sign. To evaluate the DC-bus voltage control performances, the *DC-bus* voltage reference is fixed at four levels: 48 V (from 0 to 35 s), 60 V (38 s to 70 s), 100 V (100 s to 105 s) and 48 V (105 s to 120 s) as plotted in Fig. 12. This curve shows that the proposed control strategy is satisfactory for HEV behavior simulations, and the measured voltage $V_{DC\text{-}bus}$ is very close to reference ones ($V_{DC\text{-}busref}$). These simulations results show that DC-bus voltage is related to battery's voltage as illustrated in Fig. 13, but it has less influence compared to supercapacitors ones. Load current profile obtained from Eq. (7) is plotted in Fig. 14. This current is shared between supercapacitors and battery through two DC/DC converters. Fig. 15 presents the battery's contribution on DC-bus. This current is affected by the DC-bus voltage variation, due to dependence between battery's voltage and that of the DC-bus. Fig. 16 presents the supercapacitors contribution on DC-bus. The zoomed section of this figure enables to conclude that the proposed control is satisfactory and the measured current I_{scout} is very close to reference current $I_{scout\text{-}ref}$. This dynamic behavior of the SC (charge and discharge) as function of the load current is an interesting solution to improve battery lives. In other words, this curve shows the advantages of SC in load's power smoothing.

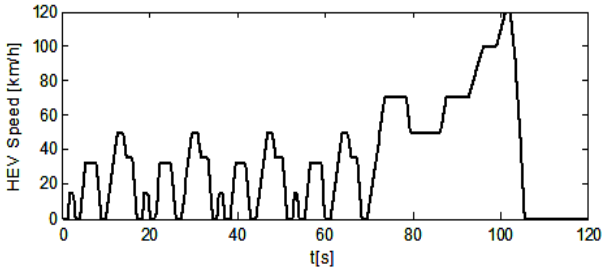

Fig. 10 Hybrid electric vehicles speed in km/h.

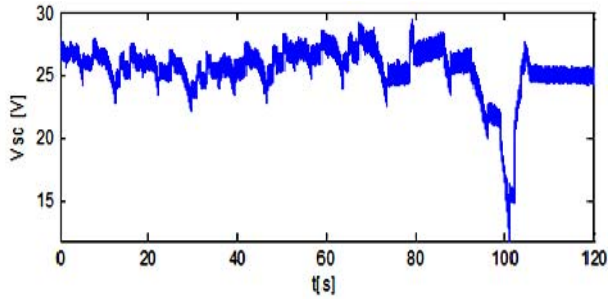

Fig. 11 Supercapacitors module voltage.

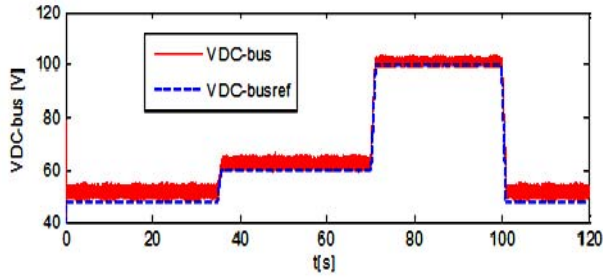

Fig. 12 DC-bus voltage control result.

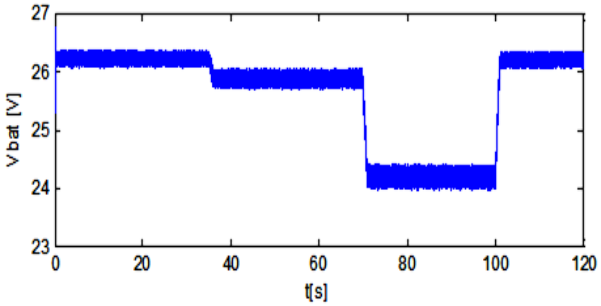

Fig. 13 Measured voltage of the battery.

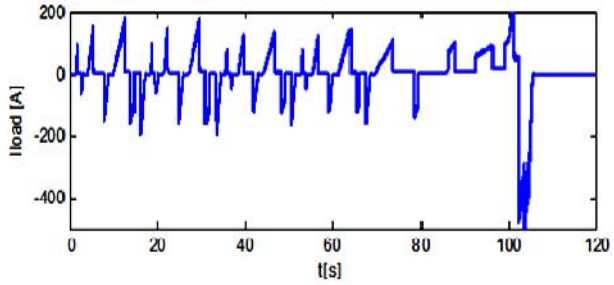

Fig. 14 Load current estimated from HEV speed in (km/h).

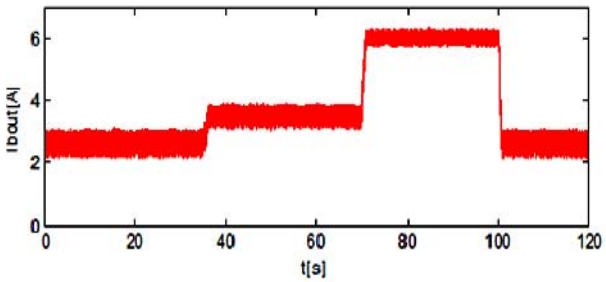

Fig. 15 Battery's contribution on DC-bus through boost converter.

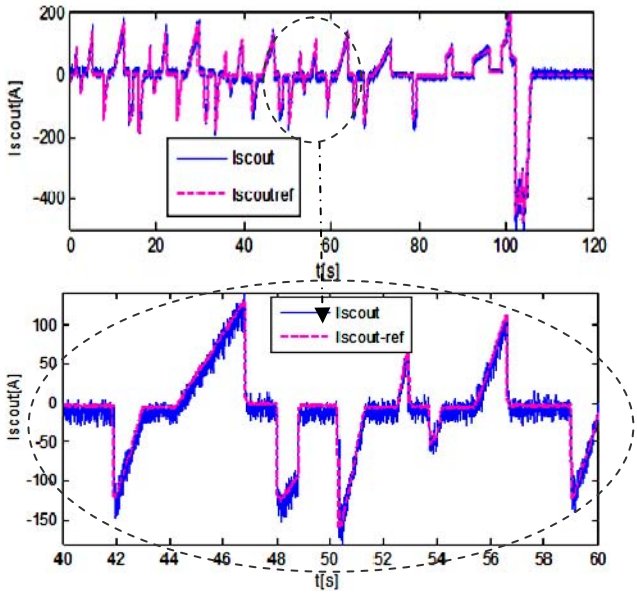

Fig. 16 SC contribution on DC-bus through buck-boost converter.

From Figs. 15 and 16, it is possible to conclude that the all fluctuations of the load current are mitigated by the SC, and this solution enables to reduce the cycle number (charge and discharge) of the battery to improve their live time.

These results show that the main contribution of the storage devices is ensured by the supercapacitors module [4, 18]. The zoomed section of the SC contribution on DC-bus shows that the proposed control strategy for SC current management is satisfactory for hybrid system behavior simulation. These simulations results enable to conclude the polynomial controller is very performing for HEV behavior simulation. This strategy will be implemented in PIC18F4431 microcontroller, for experimental test bench management in reduced scale.

6. Design and Experimental Results

6.1 Experimental Setup

Due to cost and safety reasons, an experimental test bench is carried out in reduce scale (2.7 kW), to validate the proposed control method outlined above. The designed experimental test bench includes a module of supercapacitors (20 cells in series with a maximum voltage of 54 V), a battery module with rated voltage of 24 V, a power electronic load, DC/DC converters, which ensure the energy management between the battery and supercapacitors. The described control of the DC/DC converters integrating the SC voltage limitation algorithm is implemented in PIC18F443 microcontroller. For these experimental tests, the SC module voltage is limited at 18 V (for low level) and 28 V (for high level). Due to available electronic load performances (no bidirectional), it is no possible to do the HEV current profile as presented in Fig. 14.

6.2 Experimental Results

For experimental tests, the DC-bus voltage reference is fixed at 50 V and I_{out} currents is considered negative during the SC module charge, and positive during the discharge. The charging mode corresponds to supercapacitors energy storage ($I_{out} < 0$), and that of the discharge corresponds to traction mode (SC energy supply to *DC-bus*, $I_{out} > 0$).

Fig. 17 presents DC-bus voltage; this curve enables to conclude that the implemented algorithm is satisfactory for the DC-bus voltage monitoring. However, this last is related to battery's voltage but independent to supercapacitors module voltage as plotted in Figs. 18a and 18b.

Fig. 19 presents the power electronics load (HEV emulator) current, for $I_{load} = 0$, i.e. from 0 to 111 seconds, the SC module stores energy from the battery until the high level limit (28 V). For SC discharge mode, i.e. between 111 and 178 seconds, I_{load} is fixed at 54 A. In this condition, the SC module provide hybrid vehicle energy request through the buck-boost converters. Figs. 20a and 20b shows the SC and battery contributions on DC-bus through the boost converter for the battery, and buck-boost converter for the supercapacitors.

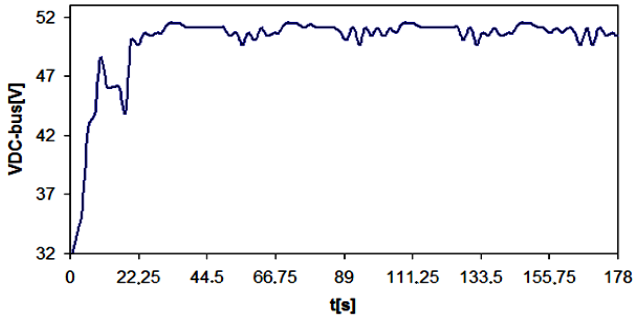

Fig. 17 DC-bus voltage.

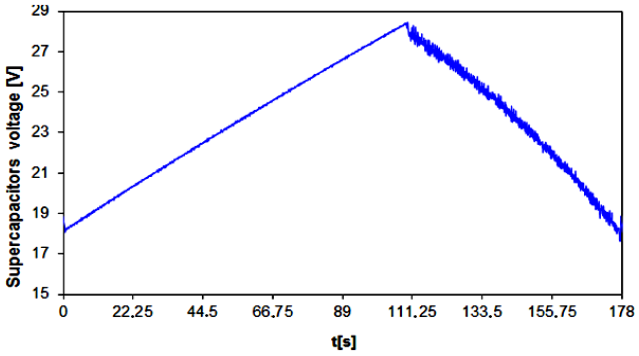

(a)

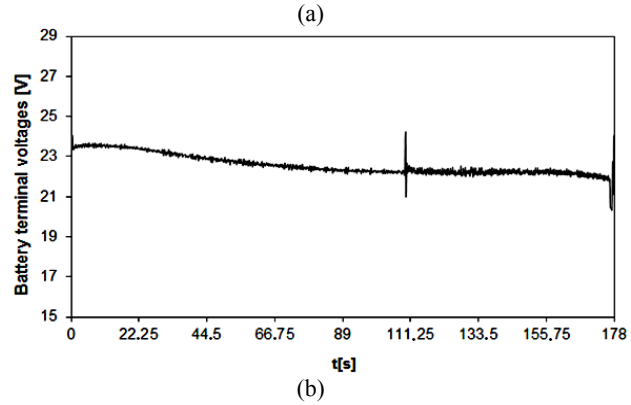

(b)

Fig. 18 (a) Measured voltage on the supercapacitors (V_{sc}); (b) Battery terminal voltage (V_{bat}).

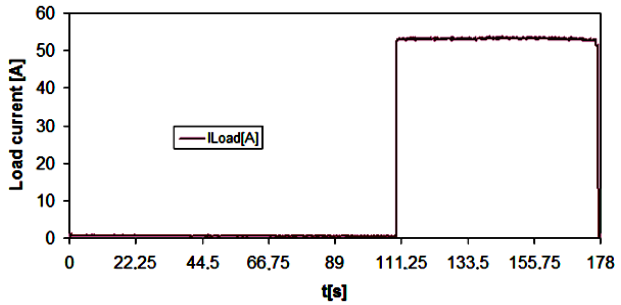

Fig. 19 Electric load current (HEV emulator).

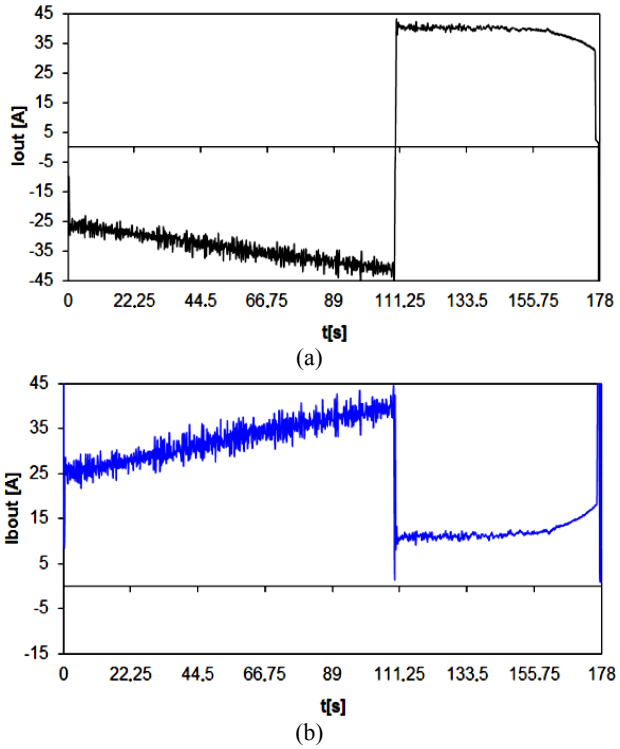

Fig. 20 (a) Measured current on the DC-bus from the supercapacitors; (b) Measured current on the DC-bus from the battery.

These experimental results enable to conclude that the proposed control for power electronics load current sharing between supercapacitors and battery is satisfactory for hybrid electric vehicles behavior simulations.

7. Conclusions

This paper presents the supercapacitors modeling based on polynomial capacitor which reflects the SC cells energy behavior during traction, and energy recovery (charge and discharge) modes.

The polynomial control method is applied to DC/DC converters to ensure the energy management between supercapacitors and battery. The resulting algorithms are interesting and effortless to implement in a microcontroller or DSP.

The supercapacitors-battery energy exchange through DC/DC converters is simulated, and experimented. Simulation, and experimental results based on polynomial controller's techniques are presented and analyzed. The performances in terms of energy management are illustrated, and the supercapacitors compensate the load power fluctuations during the transient states.

References

[1] K. Jin, X.B. Ruan, M.X. Yang, M. Xu, A hybrid fuel cell power system, IEEE Trans. on Industrial Electronics 56 (4) (2009) 1212-1222.

[2] J. Moreno, M.E. Ortuzar, J.W. Dixon, Energy-management system for a hybrid electric vehicle, using ultracapacitors and neural networks, IEEE Trans. on Ind. Elec. 53 (2) (2006) 614-623.

[3] M.B. Camara, H. Gualous, F. Gustin, A. Berthon, Design and new control of DC/DC converters to share energy between scap and battery in hybrid vehicle, IEEE Trans. on Vehicular Technology 57 (5) (2008) 2721-2735.

[4] F. Baalbergen, P. Bauer, J.A. Ferreira, Energy storage and power management for typical 4Q-load, IEEE Trans. on Industrial Electronics 56 (5) (2009) 1485-1498.

[5] M.B. Camara, D. Fodorien, H. Gualous, D. Bouquain, A. Miroui, Hybrid sources control for electric drives traction applications, in: 19th IEEE Int. Symposium on Power Electronics, Electrical Drives, Automation and Motion, Ischia, Italy, June 11-13, 2008.

[6] M.B. Camara, H. Gualous, F. Gustin, A. Berthon, B. Dakyo, DC/DC converters design for supercapacitors and battery power management in hybrid vehicle applications-polynomial control strategy, IEEE Trans. on Industrial Electronics 57 (2) (2010) 587-597.

[7] P. Thounthong, S. Raël, B. Davat, Control algorithm of fuel cell and batteries for distributed generation system, IEEE Trans. on Energy Conversion 23 (1) (2008) 148-155.

[8] M.B. Camara, F. Gustin, H. Gualous, A. Berthon, Energy management strategy for coupling supercapacitors and batteries with DC-DC converters for hybrid vehicle applications, in：13th IEEE Int. Power Electronics and Motion Control Conf. (EPE-PEMC 2008), Poland, Sep. 1-3, 2008.

[9] S.Y. Choe, J.W. Ahn, J.G. Lee, S.H. Baek, Dynamic simulator for a PEM fuel cell system with a PWM DC/DC converter, IEEE Trans. on Energy Conversion 23 (2) (2008) 669-680.

[10] P. Thounthong, S. Rael, B. Davat, Control strategy of fuel cell and supercapacitors association for a distributed generation system, IEEE Trans. on Ind. Elec. 54 (6) (2007) 3225-3233.

[11] M.B. Camara, F. Gustin, H. Gualous, A. Berthon, Supercapacitors and batteries powers management for hybrid vehicles applications, using multi boost and multi full bridge converters, in: 12th European Conf. on Power

Electronics and Applications EPE 2007, Denmark, Sept. 2-5, 2007.

[12] A. Haddoun, M.E.H. Benbouzid, D. Diallo, R. Abdessemed, J. Ghouili, K. Srairi, Modeling, analysis, and neural network control of an EV electrical differential, IEEE Trans. on Ind. Elec. 55 (6) (2008) 2286-2294.

[13] A. Haddoun, M.E.H. Benbouzid, D. Diallo, R. Abdessemed, J. Ghouili, K. Srairi, Sliding mode control of EV electric differential system, in: Proc. ICEM'06, Chania, Greece, Sept. 2006.

[14] L.I. Doré, L. Jochen, R. Daniel, B. Jean, Robust control of a 360° flexible arm using the combined pole placement/sensitivity function shaping method, IEEE Transaction on Control Systems Technology 4 (4) (1996) 369-383.

[15] M.B. Camara, H. Gualous, F. Gustin, A. Berthon, Experimental study of buck-boost converters with polynomial control strategy for hybrid vehicles applications, International Review of Electrical Engineering (IREE) 2 (1) (2007) 601-611.

[16] Y.M. Gao, M. Ehsani, Design and control methodology of plug-in hybrid electric vehicles, IEEE Trans. on Indus. Electronics 57 (2) (2010) 633-640.

[17] N.D. Benavides, P.L. Chapman, Mass-optimal design methodology for DC/DC converters in low-power portable fuel cell applications, IEEE Trans. on Power Electronics 23 (3) (2008) 1545-1555.

[18] M. Uzunoglu, M.S. Alam, Modeling and analysis of an FC/UC hybrid vehicular power system using a novel-wavelet-based load sharing algirithm, IEEE Trans. on Energy Conversion 23 (1) (2008) 263-272.